Check for updates

View Article Online
View Journal

ChemComm

Chemical Communications

Accepted Manuscript

This article can be cited before page numbers have been issued, to do this please use: Q. Wang, S. Chen, J. Jiang, J. Liu, J. Deng, X. Ping and Z. Wei, *Chem. Commun.*, 2020, DOI: 10.1039/C9CC09423G.

Volume 54
Number 1
4 January 2018
Pages 1-112

ChemComm
Chemical Communications
rsc.li/chemcomm

ISSN 1359-7345

ROYAL SOCIETY OF CHEMISTRY

COMMUNICATION
S. J. Connon, M. O. Senge *et al.*
Conformational control of nonplanar free base porphyrins: towards bifunctional catalysts of tunable basicity

This is an Accepted Manuscript, which has been through the Royal Society of Chemistry peer review process and has been accepted for publication.

Accepted Manuscripts are published online shortly after acceptance, before technical editing, formatting and proof reading. Using this free service, authors can make their results available to the community, in citable form, before we publish the edited article. We will replace this Accepted Manuscript with the edited and formatted Advance Article as soon as it is available.

You can find more information about Accepted Manuscripts in the Information for Authors.

Please note that technical editing may introduce minor changes to the text and/or graphics, which may alter content. The journal's standard Terms & Conditions and the Ethical guidelines still apply. In no event shall the Royal Society of Chemistry be held responsible for any errors or omissions in this Accepted Manuscript or any consequences arising from the use of any information it contains.

ROYAL SOCIETY
OF CHEMISTRY

rsc.li/chemcomm

View Article Online
DOI: 10.1039/C9CC09423G

COMMUNICATION

Manipulating the Surface Composition of Pt-Ru Bimetallic Nanoparticles to Control the Methanol Oxidation Reaction Pathway

Received 00th January 20xx,
Accepted 00th January 20xx

DOI: 10.1039/x0xx00000x

Qingmei Wang[a], Siguo Chen[a*], Jian Jiang[b], Jinxuan Liu[b], Jianghai Deng[a], Xinyu Ping[a], Zidong Wei[a*]

The rational manipulation of reaction intermediates is crucial to achieving high performance heterogeneous catalysis. Herein, using the *in-situ* Fourier transform infrared-diffuse reflection (FTIR) analysis, we report that the methanol oxidation reaction (MOR) intermediates can be controlled by precisely tuning the location and content of Ru on PtRu alloy surface.

Direct methanol fuel cells (DMFCs) are one of the most promising electrochemical energy conversion devices for its easy storage, delivery and refueling.[1,2] However, the extensive commercialization of DMFCs is appreciably restricted by the sluggish dynamics of the methanol oxidation reaction (MOR) and the suppressed anti-CO poisoning ability. Currently, Pt has attracted the most attentions in the field of electrocatalysis as its high kinetic rates of methanol dehydrogenation.[3,4] Unfortunately, pure Pt are severely poisoned by the adsorbed carbon monoxide (ads-CO) intermediate in MOR.[5-7] Therefore, considerable recent research efforts have been devoted to the development of high anti-CO poisoning ability electrocatalysts for MOR, especially bimetallic Pt-M alloys (M=Ru, Fe, Co, Cu, Ni, etc.) with various morphologies, composition and structures.[8]

Among which, the best-performing anti-CO poisoning catalysts for MOR is found to be bimetallic PtRu alloy, in which Pt sites are needed for methanol dehydrogenation and Ru sites are demanded for water activation. Since the catalytic process of MOR takes place on only a few layers of atoms or near the catalyst surface.[9] Achieving the atomic-level control of the surface composition and atomic arrangement is of great interest to enhance overall MOR performance of PtRu catalyst. However, it is not an easy task by the current and primary traditional wet-chemistry synthesis methods, such as chemical precipitation, impregnation, colloidal, microemulsion, polyol method, etc.[10-12] The most important challenges in these synthesis methods are the diverse nucleation and growth rates owing to the different reduction potential of Pt ($[PtCl_4]^{2-}+2e^- \leftrightarrow Pt+4Cl^-, E_0=+0.73V$)and Ru ($Ru^{2+}+2e^- \leftrightarrow Ru$, $E_0=+0.45V$), which unavoidably result in alloy inhomogeneity and low alloy degree because of the low temperature synthesis conditions.[13,14] Consequently, further step of high temperature procedure is necessarily required to improve the alloy homogeneity and alloy degree, which inevitably leads to nanoparticles (NPs) growth, sintering and aggregation.[15] To overcome these elusive challenges and achieve both high MOR activity and anti-CO poisoning ability in DMFCs applications, therefore, the exploration of simple and cost-efficient methodologies for fabricating PtRu alloys with uniform sizes, preferable alloying degree and controlled compositions is highly acceptable.

Herein, we reported that the pathway of MOR on Pt-Ru alloy can be controlled by precisely manipulating the surface composition of Pt-Ru bimetallic NPs. We tune the location and content of Ru on PtRu alloy surface through a thermally driven interfacial diffusion route that allows for selectively transforming the solid Pt NPs supported on carbon (Pt/C) into Pt-rich PtRu alloy, Ru-rich PtRu alloy and PtRu alloy with moderate surface atom ratio of Pt to Ru. As shown in Figure 1, the high-temperature, in junction with the H_2/N_2 reduction atmosphere, drives the “reduction” and “diffusion” of absorbed Ru^{3+} into the Pt to form PtRu alloy. We also correlated their MOR pathway and activity with the location and content of Ru in PtRu alloy by applying *in-situ* Fourier transform spectrum (FTIRs) infrared-diffuse

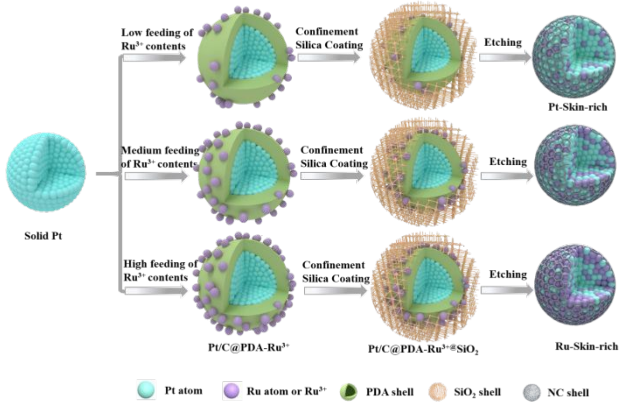

Figure 1 The synthetic overall concept of the Pt-skin-rich $Pt_1Ru_{0.5}$@NC/C, moderate Pt and Ru content Pt_1Ru_1@NC/C and Ru-skin-rich Pt_1Ru_2@NC/C samples.

---

a The State Key Laboratory of Power Transmission Equipment & System Security and New Technology, Chongqing Key Laboratory of Chemical Process for Clean Energy and Resource Utilization, School of Chemistry and Chemical Engineering, Chongqing University, Chongqing 400044, China.
E-mail: csg810519@126.com; zdwei@cqu.edu.cn
b The State Key Laboratory of Fine Chemical Industry, Dalian University of Technology, Dalian, China

Electronic Supplementary Information (ESI) available: See DOI: 10.1039/x0xx00000x

View Article Online
DOI: 10.1039/C9CC09423G

reflection spectrum (FTIRs). Our insights establish that the Pt-rich PtRu alloy catalyst featured a MOR pathway through $HCOO^-$ intermediate, while the Ru-rich PtRu alloy catalyst exhibit a CO intermediate pathway. Meanwhile, the PtRu alloy catalyst with optimal surface atom ratio of Pt to Ru, which possess the best MOR activity and anti-CO poisoning ability, convey a combined pathway of $HCOO^-$ and CO intermediate.

The PtRu alloy with different Ru contents was prepared by integrating the thermal-driven structural evolution and surface manipulating strategies.[16] The resultant PtRu alloy samples were represented as "Pt_1Ru_x/C@NC", where "X" indicates the feeding molar ratio of Ru^{3+} to Pt ($Pt_1Ru_{0.5}$/C@NC, Pt_1Ru_1/C@NC, Pt_1Ru_2/C@NC, respectively). The morphology and structure of the as-prepared PtRu alloy were first investigated by transmission electron microscopy (TEM). No noticeable Pt conglomeration happened in the $Pt_1Ru_{0.5}$/C@NC (Figure S1a), Pt_1Ru_1/C@NC (Figure S1d) and Pt_1Ru_2/C@NC (Figure S1g), suggesting that the agglomeration of the PtRu NPs can be effectively prevented by our reported composite procedure as compared to the commercial PtRu/C catalyst (Figure S2). As shown in Figure S1c, 1f, 1i, it is obvious that with the increase in the Ru content, the average particle size of PtRu gradually increased from 2.60 nm for $Pt_1Ru_{0.5}$/C@NC to 2.72 nm for Pt_1Ru_1/C@NC and 3.04 nm for Pt_1Ru_2/C@NC, indicating that more Ru have been diffusion into Pt due to the increased feeding Ru^{3+} contents. The Ru contents in the as-prepared PtRu samples were further confirmed by the inductively coupled plasma mass spectrometry (ICP-MS) analysis. As shown in Table S1, the Ru content in PtRu alloy gradually increased from 0.8% for $Pt_1Ru_{0.5}$/C@NC to 2.1% for Pt_1Ru_1/C@NC and 3.9% for Pt_1Ru_2/C@NC, further confirming that the Ru content in PtRu alloy can be controlled by tuning the feeding of Ru^{3+} content. The crystal structure of the as-prepared PtRu alloy was investigated by the powder X-ray diffraction (XRD). As shown in Figure 2a, the peak position of the $Pt_1Ru_{0.5}$/C@NC, Pt_1Ru_1/C@NC and Pt_1Ru_2/C@NC shifted to high angles as compared to the pure Pt (PDF#04-0802), further confirming that the pre-adsorbed Ru^{3+} has been successfully reduced and diffused into Pt lattice to form bimetallic PtRu alloy. The induced strain variations of $Pt_1Ru_{0.5}$/C@NC, Pt_1Ru_1/C@NC and Pt_1Ru_2/C@NC catalysts which based on the Bragg's law and the peak position of Pt (111) are 1.49%, 1.66% and 1.13%, respectively (Table S2). The different crystal lattice shrink degree was also confirmed by high-resolution TEM (HRTEM), in which the degree of crystal lattice shrinkage on Pt_1Ru_1/C@NC (Figure S1b) is higher than $Pt_1Ru_{0.5}$/C@NC (Figure S1e) and Pt_1Ru_2/C@NC (Figure S1h), respectively. This result means that higher Ru feeding content would not consequently result in higher alloying degree. The possible reason is due to the inhomogeneity of the distribution of Ru in the whole PtRu NPs. The composition profiles of the as-prepared PtRu alloy were further characterized by atomically resolved aberration-corrected high-angle annular dark-field scanning TEM (HAADF-STEM) and the energy-dispersive X-ray spectroscopy (EDX) in combination with the energy loss spectroscopy (EELS) line scan analysis. As shown in Figure 2f, 2g, 2n, the overall elemental mapping images reveal that most of the Ru are located on the surface of the PtRu NP for thorough of the as-prepared PtRu samples. Further EELS analysis results (Figure 2g, 2k, 2o) show that the lower feeding molar ratios of Ru^{3+} to Pt are beneficial to the formation of Pt-skin-rich PtRu alloy phases ($Pt_1Ru_{0.5}$/C@NC) with the Ru/Pt molar ratio of 0.2, while the higher feeding molar ratios of Ru^{3+} to Pt led to the formation of a Ru-skin-rich PtRu alloy (Pt_1Ru_2/C@NC) with the Ru/Pt molar ratio of 0.5. For comparison, the medium feeding molar ratios of Ru^{3+} to Pt prefer to form homogenous Ru distribution in whole Pt_1Ru_1/C@NC alloy (Figure 2h, 2l, 2p). These results are firmly certificating that the location and composition of Ru at PtRu NPs can be exactly manipulated by altering the feeding of Ru^{3+} content, which is consistent with the analysis of XRD and ICP. Additional representative HAADF-STEM and elemental mapping images of Pt_1Ru_1/C@NC are shown in Figure S3 and Figure S4.

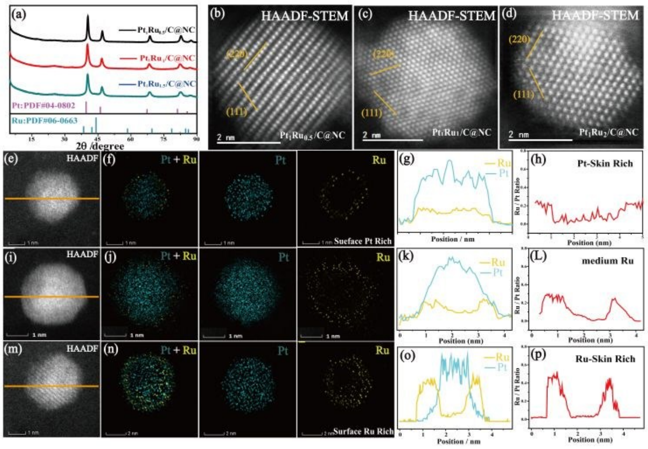

Figure 2 The powder X-ray diffraction of $Pt_1Ru_{0.5}$@NC/C, Pt_1Ru_1@NC/C and Pt_1Ru_2@NC/C catalysts (a) and the Aberration-corrected HAADF-STEM images, its corresponding EDX elemental mapping and EELS images as well as the calculated Ru/Pt atomic ratios of the $Pt_1Ru_{0.5}$@NC/C (e-h), Pt_1Ru_1@NC/C (i-l) and Pt_1Ru_2@NC/C (m-p) catalysts, respectively.

The surface composition and chemical status of the PtRu samples were further investigated by X-ray photoelectron spectroscopy (XPS). As shown in Figure S5, the presence and the corresponding content of Pt, Ru, C, N and O in PtRu samples were confirmed by the XPS survey, respectively. The atomic ratio of the Ru: Pt in the PtRu surface gradually increased from 1.68 for $Pt_1Ru_{0.5}$/C@NC to 3.02 for Pt_1Ru_1/C@NC and 19.42 for Pt_1Ru_2/C@NC, respectively, further indicating the surface Ru contents in PtRu alloy consequently increased with the raise of the feeding of Ru^{3+} contents. The peaks of the N1s signals in PtRu samples could be deconvoluted into pyridinic-N (398.21 eV), pyrrolic-N (400.54 eV) and quaternary-N (401.20 eV), demonstrating that dopamine precursor has been transformed into NC layer (Figure S6). The peak at 280.6 eV represents the metallic Ru, and the peaks at 281.3 and 281.8 eV indicate the Ru oxides (Figure S7). Moreover, the Pt $4f_{7/2}$ and Pt $4f_{5/2}$ peaks of the homemade PtRu sample can be split into predominant metallic Pt and Pt oxides (Figure S8), which can provide more effective active sites for MOR. The electron transfer degree from Ru to Pt in Pt_1Ru_x/C@NC samples was determined by the negative shift value in the Pt $4f_{7/2}$ peak as compared with the Pt/C catalyst (Figure 3a), which followed an order of 0.60eV (Pt_1Ru_1/C@NC), 0.34eV ($Pt_1Ru_{0.5}$/C@NC) and 0.24eV(Pt_1Ru_2/C@NC), respectively. The lower negative shift in $Pt_1Ru_{0.5}$/C@NC and Pt_1Ru_2/C@NC catalysts are owing to the inhomogeneity of the electronic donor Ru and the electronic acceptor Pt (Figure 3b).[17] To

View Article Online
DOI: 10.1039/C9CC09423G

further evaluate the effect of Ru content on anti-CO poisoning ability of the PtRu sample, the CO-stripping experiment were conducted. As shown in Figure 3c, the Pt_1Ru_1/C@NC shows the lowest onset potential of the CO oxidation as compared with $Pt_1Ru_{0.5}$/C@NC, Pt_1Ru_2/C@NC and commercial Pt/C catalysts, suggesting that the Pt_1Ru_1/C@NC exhibit accelerated CO oxidation kinetics respect to its counterpart. As confirmed by XPS, the homogeneity of Ru in Pt_1Ru_1/C@NC catalyst can induce more electron transfer from Ru to Pt as compared with $Pt_1Ru_{0.5}$/C@NC, Pt_1Ru_2/C@NC, which will weaken the Pt-CO adsorption energy and facilitate the removal of ads-CO on Pt sites, resulting in improving the anti-CO poisoning ability of the catalysts.[18] The specific value of electrochemical surface area (ECSA) based on the CO oxidation charge and Pt mass for the $Pt_1Ru_{0.5}$/C@NC is estimated to be 49 m^2/g_{Pt} (Figure 3d), which is slightly higher than the Pt_1Ru_1/C@NC (47 m^2/g_{Pt}) and Pt_1Ru_2/C@NC (39 m^2/g_{Pt}) catalysts. It is suggesting that the more Ru feeding, the less Pt active sites for MOR in catalyst are exposed.[19]

The MOR activity was further evaluated by the cyclic voltammetry (CV) in N_2-saturated 0.1 M $HClO_4$ solution containing 0.5M CH_3OH. As shown in Figure 3e, the peak currents of MOR are found to be 5.29, 5.31 and 2.20 $mA.cm^{-2}$ on the $Pt_1Ru_{0.5}$/C@NC, Pt_1Ru_1/C@NC and Pt_1Ru_2/C@NC catalysts, respectively (Figure 3f). The higher forward peak current on Pt_1Ru_1/C@NC catalyst indicating that the faster dynamics rate of C-H cleavage of methanol. To gain further insights into the MOR activity of PtRu samples, the peak current at $0.7V_{RHE}$ correlated with MOR in the forward scan is normalized with respect to both ECSA and the loading amount of Pt. As shown in Figure 3g and Table S3, the MOR specific activity firstly increased with the increase of Ru surface composition from 1.29 $mA.cm^{-2}$ for $Pt_1Ru_{0.5}$/C@NC to 1.36 $mA.cm^{-2}$ for Pt_1Ru_1/C@NC and subsequently decreased with further increases of Ru surface composition to 0.59 $mA.cm^{-2}$ for Pt_1Ru_2/C@NC. The mass activities gradually increased from 0.59 mA/ug_{Pt} for $Pt_1Ru_{0.5}$/C@NC to 0.67 mA/ug_{Pt} for Pt_1Ru_1/C@NC and then decreased to 0.23 mA/ug_{Pt} for Pt_1Ru_2/C@NC, respectively. Except for the peak current, the value of I_f/I_b (I_f and I_b are represent the forward and backward current density) is also very important factor to evaluate the anti-CO poisoning ability. The Pt_1Ru_1/C@NC catalyst exhibits the higher I_f/I_b value of 7.17 than that of the $Pt_1Ru_{0.5}$/C@NC (6.86) and Pt_1Ru_2/C@NC (5.46) catalysts, respectively. The higher I_f/I_b ratio and forward peak current propose that the methanol would be effectively oxidized during the forward potential scan and there would be generate less ads-CO species during the backward potential scan, thereby the catalyst of Pt_1Ru_1/C@NC maintain superior MOR activity and anti-CO poisoning ability (Figure S9 and Scheme S2). To the best of our knowledge, these values including the I_f/I_b, the mass activity and the specific activity are advantageous to those of other PtRu catalysts reported to date as MOR catalysts in an acid surroundings (Table S4). The stability towards MOR in the $Pt_1Ru_{0.5}$/C@NC, Pt_1Ru_1/C@NC and Pt_1Ru_2/C@NC catalysts was conducted by the chronoamperometric (CA) on a constant potential of $0.7V_{RHE}$ for 7500s. The polarization currents in $Pt_1Ru_{0.5}$/C@NC, Pt_1Ru_1/C@NC and Pt_1Ru_2/C@NC are decrease at the primary stage (Figure 3h), which is mainly owing to the formation of the by-product and intermediate species (Scheme S2) during MOR.[24] However, the density of the anodic current of the Pt_1Ru_1/C@NC is always higher than the $Pt_1Ru_{0.5}$/C@NC and Pt_1Ru_2/C@NC during the entire time range (Figure 3i). Moreover, Figure S10 also indicating that the change in particle size is negligible in the Pt_1Ru_1/C@NC samples after long-term cycles, whereas obvious aggregation occurs on the Pt_1Ru_2/C@NC catalysts under the same conditions. These results again confirm that the Pt_1Ru_1/C@NC sample with the homogeneity distribution of Ru contents on the surface possess better anti-CO poisoning ability and improved stability in MORs (Figure S11). Therefore, combined with the ICP-MS after the stability test (Table S1), we can conclude that the appropriative surface Pt and Ru composition can effectively prevent the PtRu NPs from aggregation and subsequently promote the electrochemical stability during potential cycling.

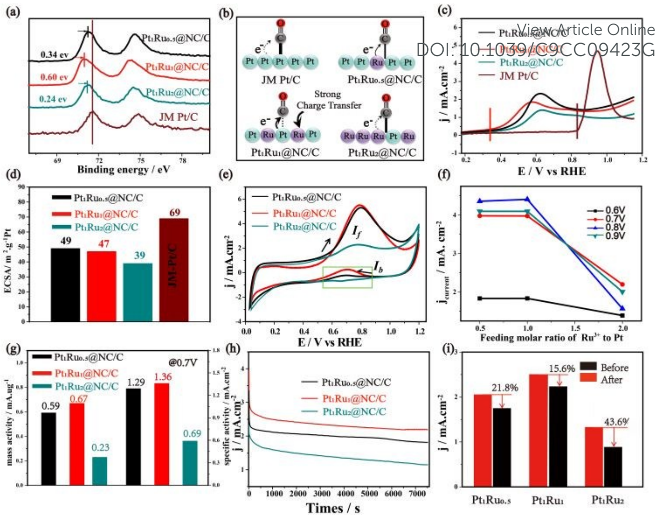

Figure 3 (a) XPS Pt 4f scans of $Pt_1Ru_{0.5}$@NC/C, Pt_1Ru_1@NC/C and Pt_1Ru_2@NC/C catalysts as compared with the primitive Pt/C catalysts and (b) the corresponding illustration of the electron transfer when CO adsorbed on the surface. (c) CO stripping curves of the $Pt_1Ru_{0.5}$@NC/C, Pt_1Ru_1@NC/C, Pt_1Ru_2@NC/C and Pt/C catalysts and (d) corresponding ECSA s well as (e) the CV curves and peak current (f) in 0.1 M $HClO_4$ + CH_3OH solution. (g) The mass and specific activity at peak potential and the chronoamperometric on a constant potential of $0.75V_{RHE}$ for 7500s (h) and the current density descend percentage of the $Pt_1Ru_{0.5}$@NC/C, Pt_1Ru_1@NC/C and Pt_1Ru_2@NC/C catalysts (i).

To get an insight into how the MOR activity trajectories of correlate with Pt and Ru compositional changes, the *in-situ* Fourier transform infrared-diffuse reflection spectroscopy (FTIRs) was performed.[20-24] For Pt-rich $Pt_1Ru_{0.5}$@NC/C catalyst, the characteristic adsorbed peak related to methyl formate ($HCOOCH_3$) intermediate can be clearly observed at 1260 cm^{-1} with the increasing of scan potential, while the bands of CO linear molecules (CO_L) which represent the CO pathway are not observed, indicating that the $Pt_1Ru_{0.5}$@NC/C catalyst achieving MOR through $HCOO^-$ intermediate pathway (Figure 4a, 4d). On the contrary, the characteristic adsorbed peak of CO_L is evidently viewed at 2050 cm^{-1} in Ru-rich Pt_1Ru_2@NC/C catalyst, while the bands of $HCOOCH_3$ are not observed, indicating that the Pt_1Ru_2@NC/C catalyst achieving MOR through CO pathway (Figure 4c, 4f). Different from the solely MOR pathway in Pt-skin-rich $Pt_1Ru_{0.5}$@NC/C and Ru-skin-rich Pt_1Ru_2@NC/C samples, the Pt_1Ru_1@NC/C catalyst demonstrate a mixed pathway through $HCOO^-$ and CO intermediate (Figure 4b, 4e), in which both the characteristic peak of $HCOOCH_3$ and CO_L are obviously found.[25-29] By correlating the

View Article Online
DOI: 10.1039/C9CC09423G

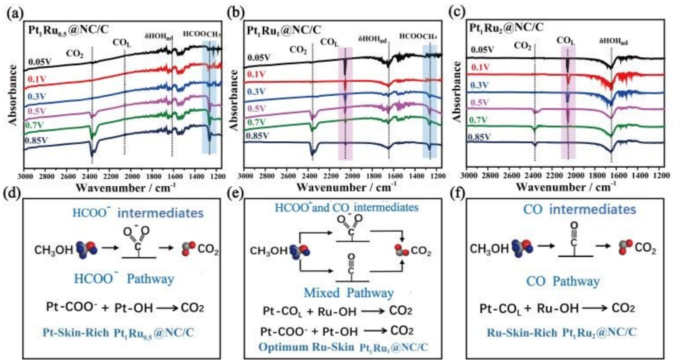

Figure 4 *In-situ* FTIR spectra for methanol oxidation in 0.1 M $HClO_4$ + CH_3OH solution after 100s on $Pt_1Ru_{0.5}$@NC/C (a), Pt_1Ru_1@NC/C (b) and Pt_1Ru_2@NC/C (c) and the corresponding schematic illustration of the MOR on $Pt_1Ru_{0.5}$@NC/C (d), Pt_1Ru_1@NC/C (e) and Pt_1Ru_2@NC/C (f).

surface Pt and Ru contents with MOR activity and reaction pathway, we can conclude that a relatively low or high surface Ru content is not beneficial to the MOR. This phenomenon can be explained by the famous Watanabe-Motoo bifunctional mechanism, in which the insufficient Ru in $Pt_1Ru_{0.5}$@NC/C catalyst cannot effectively remove the CO species, while the redundant of Ru in Pt_1Ru_2@NC/C catalyst would result in a relative low number of active Pt sites for the methanol dehydrogenation. The Pt_1Ru_1@NC/C catalyst with the optimum Ru and Pt content on the surface can balance these composition-dependent ensemble effects, which synchronously promote the MOR activity and anti-CO poisoning ability. Other representative *in-situ* FTIR spectra of the as-prepared PtRu alloy at different time were displayed in the supporting information, respectively (Figure S12-S16).

In conclusion, we successfully prepared three types of PtRu catalyst with Pt-rich $Pt_1Ru_{0.5}$/C@NC alloy, Ru-rich Pt_1Ru_2/C@NC alloy and Pt_1Ru_1/C@NC alloy with optimal surface atom ratio of Pt to Ru. According to the *in-situ* FTIRs, we observed that the $Pt_1Ru_{0.5}$/C@NC achieving MOR through $HCOO^-$ intermediate pathway, while the Pt_1Ru_2/C@NC catalyst attainting MOR through CO intermediate pathway. Meanwhile, the Pt_1Ru_1/C@NC with an optimal ratio of Ru to Pt on the surface can achieve the best performance of MOR activity and anti-CO poisoning ability through a mixed pathway of $HCOO^-$ and CO intermediates. Our work demonstrates the significance of surface composition control at the atomic-level and reveals an avenue for the exploration of highly active bimetallic nanoparticles for electrochemical energy conversion.

Conflicts of interest

There are no conflicts to declare.

Acknowledgements

This research work was financially supported by the National Key Research and Development Program of China (2016YFB0101202), National Natural Science Foundation of China (Grant No. 91534205, 21436003, 21576031 and 21776023), and by the Fundamental Research Funds for the Central Universities (2018CDXYHG0028).

References

1 L. Huang, X. P. Zhang, Y. J. Han, Q. Q. Wang, Y. X. Fang, S. J. Dong, Chem. Mater. 2017, **29**, 4557-4562.

2 H. Luo, W. J. Jiang, C. Lin, W. Dong, S. Niu, L. B. Huang, X. Zhang, Z. Wei and J. S. Hu, Chem. Commun., 2018, **54**, 8190–8193.

3 A. Hamnett, Catalysis Today 1997, **38**, 445-457.

4 J. Suntivich, Z. C. Xu, C. E. Carlton, J. Kim, B. H. Han, S. W. Lee, N. Bonnet, N. Marzari, L. F. Allard, H. A. Gasteiger, K. Hamad-Schifferli, Y. S. Horn, J. Am. Chem. Soc. 2013, **135**, 7985-7991.

5 L. Zhuang, J. Jin, Hector D. Abrun, J. Am. Chem. Soc. 2007, **129**, 11033-11035.

6 Y. C.Wei, X. X. Wu, Y. L. Zhao, L. Wang, Z. Zhao, X. T. Huang, J. Liu, J. M.Li, Applied Catalysis B: Environmental, 2018, **236**, 445-457.

7 W. Y. Chen, D. L. Li, C. Peng, G. Qian, X. Z. Duan, D. Chen, X. G. Zhou, Journal of Catalysis, 2017, **356**, 186-196.

8 X. L. Sun, D. G. Li, Y. Ding, W. L. Zhu, S. J. Guo, Z. L. Wang, S. H. Sun, J. Am. Chem. Soc. 2014, **136**, 5745-5749.

9 W. Hong, J. Wang, E. Wang, Small 2014, **10**, 3262-3265.

10 J. Liu, X. X. Wu, L. P. Yang, F. Wang, J. Yin, Electrochimica Acta, 2019, **297**, 539-544.

11 Y. N. Liu, L. R. Zheng, X. Z. Cao, Y. Man, J. T. Feng, J. A. Anderson, D. Q. Li, A. J. McCue, P. F. Yang, Y. F. He, Chem. Sci., 2019, **10**, 3556-3566.

12 K. Zhang, D. Bin, B. B. Yang, C. Q. Wang, F. F. Ren, Y. K. Du, Nanoscale, 2015, **7**, 12445-12451

13 Q. M. Wang, S. G. Chen, P. Li, S. Ibraheem, J. Li, J. H. Deng, Z. D. Wei, Applied Catalysis B: Environmental, 2019, **252**, 120-127.

14 W. Hong, J. Wang, E. Wang, Nano Research, 2015, **8**, 2308-2316.

15 Z. C. Wang, A. H. Tavabi, L. Jin, J. Rusz, D. Tyutyunnikov, H. Jiang, Y. Moritomo, J. Mayer, R. E. D. Borkowski, R. Yu, J. Zhu, X. Y. Zhong, Nature Materials, 2018, **17**, 221-225.

16 W. Y. Zhang, Y. Yang, B. L. Huang, F. Lv, K. Wang, N. Li, M. C. Luo, Y. G. Chao, Y. J. Li, Y. J. Sun, Z. K. Xu, Y. N. Qin, W. X. Yang, J. H. Zhou, Y. P. Du, D. Su, S. J. Guo, Adv. Mater. 2019, **31**, 1805833.

17 J. Y. Wang, Y. Cui, D. Wang, Adv. Mater. 2018, 1801993.

18 Q. M. Wang, S. G. Chen, F. Shi, K. Chen, Y. Nie, Y. Wang, R. Wu, J. Li, Y. Zhang, W. Ding, Y. Li, L. Li, Z. D. We, Adv. Mater. 2016, **28**, 10673-10678.

19 Z. Y. Wu, H. W. Liang, B. C. Hu, S. H. Yu, Angew. Chem. Int. Ed., 2018, **57**,15646 -15662.

20 W. Hong, J. Wang, E. Wang, J. Mater. Chem. A, 2015, **3**, 13642-13647.

21 Q. B. Fan, C. Pu, E. S. Smotki, J. Electrochem. Soc., 1996, **143**, 10.

22 J. Q. Xie, Y. Q. Ji, J. H. Kang, J. L. Sheng, D. S. Mao, X. Z. Fu, R. Sun, Ching-Ping Wong, Energy & Environmental Science. 2019, **12**, 194-205.

23 H. Gong, S. G. Sun, Y. J. Chen, S. P. Chen, J. Phys. Chem. B 2004, **108**, 11575-11584.

24 K. Walter, O. V. Buyevskaya, D. Wolf, M. Baerns, Catalysis Letters, 1994, **29**, 261-270.

25 P. Z. Chen, Y. Tong, C. Z. Wu, Y. Xie, Acc. Chem. Res. 2018, **51**, 2857-2866.

26 H. W. Zhang, P. K. Shen, Chem. Rev. 2012, 112, **5**, 2780-2832.

27 K. Ma, Y. Tian, Z. J. Zhao, Q. P. Cheng, T. Ding, J. Zhang, L. R. Zheng, Z. Jiang, T. Abe, N. Tsubaki, J. L. Gong, X. G. Li, Chem. Sci., 2019, **10**, 2578-2584.

28 Q. Wang, X. Lu, Q. Xin, G. Q. Sun, Chinese Journal of Catalysis, 2014, **35**, 1394-1401.

29 J. Kaiser, L. Colmenares, Z. Jusys, R. Mörte, H. Bönnemann, G. Köhl, H. Modrow, J. Hormes, R. J. Behm, Fuel Cells, 2006, **06**, 190-202.

View Article Online
DOI: 10.1039/C9CC09423G

TOC

Here we achieve surface composition precisely manipulating of bimetallic PtRu alloy from Pt-skin-rich to Ru-skin-rich and report that the MOR pathway can be controlled by tuning the location and content of Ru on PtRu alloy surface.